International Journal of Design & Nature and Ecodynamics
Vol. 20, No. 6, June, 2025, pp. 1243-1255
Journal homepage: http://iieta.org/journals/ijdne

Synthesis, Characterization, and Evaluation of Nano MgO/bentonite Composite for Efficient AMOX Adsorption from Wastewater

Zahraa Abd Alsaheb, Khalid Khazzal Hummadi*

Department of Environmental Engineering, College of Engineering, University of Baghdad, Baghdad 10071, Iraq

Corresponding Author Email: dr.khalid.hummadi@coeng.uobaghdad.edu.iq

Copyright: ©2025 The authors. This article is published by IIETA and is licensed under the CC BY 4.0 license (http://creativecommons.org/licenses/by/4.0/).

https://doi.org/10.18280/ijdne.200606

Received: 15 May 2025
Revised: 17 June 2025
Accepted: 23 June 2025
Available online: 30 June 2025

Keywords:
adsorption, bentonite, NanoMgO, AMOX, wastewater treatment

ABSTRACT

Conventional water treatment methods often fail to remove pharmaceutical contaminants, particularly antibiotics such as amoxicillin (AMOX), with sufficient efficiency, and this shortcoming necessitates the exploration of more efficient and sustainable adsorbents. The adsorption of AMOX onto Nano magnesium oxide-bentonite composite (NMgO/bentonite) was investigated under different conditions. The NMgO/bentonite sample was characterized by Fourier transform infrared spectroscopy, powdered diffraction and surface area analysis, and electron microscopy. The assessment of the composite's adsorption ability was bolstered by these investigations, which also disclosed its morphological and surface features. The BET specific surface area increased from 37.13 for bentonite to 57.23 m^2/g for NMgO/bentonite. Removal efficiency reached 94.96% at C_0 = 80 mg/L. With a maximal capacity of 263.143 mg/g, the Langmuir model confirmed the synergistic activity of bentonite and Nano-MgO. The pseudo-second-order model described the kinetics, with a rate constant of 0.0015 g mg^{-1} min^{-1} at 25°C and an activation energy of 30.35 kJ/mol. A chemisorption-driven, spontaneous, exothermic process was revealed by thermodynamic analysis. Under these conditions, the adsorption behaviour of NMgO/bentonite verifies its applicability to the removal of pharmaceutical pollutants from water systems.

1. INTRODUCTION

The most notable contaminants in wastewater, water on the surface, and groundwater are pharmaceuticals, especially antibiotics [1]. They are generally used post-diagnosis to treat and mitigate illnesses in people, animals, and plants [2]. Both surface and subsurface water include pharmaceutical chemicals, such as antibiotics and their metabolites [3]. A significant number of pharmaceutical chemicals exhibit incomplete biodegradability and frequently display resistance to traditional wastewater treatment techniques [4]. While these compounds often linger in treated water in certain amounts, some have even filtered into tap water supplies [5]. AMOX, one of the most widely administered antibiotics and a major drug contaminant detected, has become a regular presence in aquatic settings near hospitals and pharmaceutical plants that discharge [6]. At elevated concentrations, AMOX poses health risks to both people and ecosystems. It could also foster antibiotic resistance in bacteria, making future infections harder to cure with standard drugs. The World Health Organization (WHO) continues to classify it as a core antibiotic; however, growing concerns about pharmaceutical pollution have led to new global guidelines aimed at reducing antibiotic emissions, particularly from manufacturing sources. Ongoing monitoring, better waste treatment, and responsible antibiotic use are key to minimizing these environmental risks. AMOX is a widely used antibiotic. The WHO reports focus on the broader issue of AMR and specifically concerning bacteria and resistance patterns. For these important reasons, eliminating AMOX residues from water has become a focus of research [7]. Waste generated by pharmaceutical manufacturing must undergo treatment before being released into natural ecosystems to avoid potential environmental harm. Although several approaches have been developed to address the presence of AMOX in effluents, many of these technologies remain financially burdensome [8, 9]. Techniques such as electrocoagulation, electrochemical oxidation, and advanced oxidative degradation have been utilised for this purpose, alongside adsorption-based strategies [10]. Adsorption, in particular, has emerged as a practical and efficient alternative due to its operational ease and reliable performance. Many adsorbents showed the capacity to eliminate various organic substances from water, including antibiotics, industrial dyes, toxic metals, and other hazardous pollutants [11].

The volcanic clay bentonite has a high concentration of montmorillonite and is organised as a 2:1 mineral with two silica sheets in a tetrahedral shape and an octahedral alumina sheet in the middle. Because Si^{4+} is substituted for Al^{3+} in the tetrahedral layer and Mg^{2+} or Fe^{3+} is substituted in the octahedral layer, the clay develops an overall negative surface charge [12]. Bentonite has emerged as the most efficient option due to its affordability, especially when compared to activated carbon, which requires costly preparation processes [13-15]. Study [16] reported that bentonite adsorbed 3.46 mg/g of ciprofloxacin and 245.09 mg/g of ampicillin, which

indicates its convincing adsorption capacity. In addition, natural bentonite has been employed as a carrier for both nano and non-nano materials in the treatment of such contaminants [17]. The adsorption process involves both the bentonite surface and its internal pores. Organic molecules pass through the bentonite pores, where they become trapped [18]. Modified bentonite is capable of adsorbing weakly polar organic compounds that are soluble in aqueous solutions [19]. When modified, bentonite gains a positive surface charge and strong electrostatic attraction, which facilitates interactions with quaternary amine groups. The modification replaces inorganic cations with organic ones to shift its surface properties from hydrophilic to hydrophobic and enhance its effectiveness as an adsorbent [20]. Study [21] used modified bentonite with hexadecyl trimethyl ammonium (DK1) to remove AMOX. Study [22] reported a capacity of 283.5 mg/g for tetracycline using organo-bentonite.

The use of magnesium oxide (MgO) in adsorption processes offers several advantages. Its cost is significantly lower than that of iron and manganese oxides; it has minimal environmental impact, is non-polluting, and can be easily recovered from aqueous media. For these reasons, MgO is used as an antibiotic adsorbent for its high adsorption capacity, especially under acidic conditions [23]. Treating natural bentonite with MgO enhances its AMOX removability from aqueous solutions. The improved performance results from the modified bentonite surface becoming more attractive to anionic pollutant molecules [24]. Recent studies have highlighted the application of MgO and ZnO/MgO nanocomposites in wastewater treatment. These materials showed high potential in toxic metal ions removal from contaminated water systems [25], as well as in the treatment of dye-laden effluents (i.e., Congo red) [26]. Another study looked at how well MgO nanoparticles absorbed some toxic compounds from water, including arsenic, neutral red, and bright cresyl blue [27].

As far as current literature indicates, there have been no prior investigations focused on the removal of AMOX using bentonite enhanced with nanoscale MgO. MgO nanoparticles are recognised as promising basic oxides with wide-ranging applications [28], including their use in adsorption processes, catalytic reactions, and the fabrication of refractory ceramic materials. MgO is a unique solid with a simple crystal structure, simple stoichiometry, and strong ionic character. It can be synthesized in various particle sizes and shapes. Nano crystalline MgO particles have an elevated degree of specific surface area and reactivity due to their size and shape, which are caused by an elevated number of edge and corner sites and surface imperfections, according to a previous study [29].

In order to create a novel nanocomposite adsorbent for the removal of AMOX from wastewater, the current effort aims to develop Nano-MgO (NMgO) loaded bentonite. A battery of tests was carried out to ascertain the ideal circumstances for attaining the maximum adsorption capacity. We examined absorption kinetics, as equilibrium isotherms, and thermodynamic factors to help us understand the process further.

2. METHODS AND MATERIALS

2.1 Materials

AMOX, with a 99% purity, was supplied by the Samarra Pharmaceutical Laboratory and used directly without any additional processing. Figure 1 shows its chemical structure, which is $C_{16}H_{19}N_3O_5S$. It has a molecular mass of 365.404 g/mol and an absorption peak at 272 nm. Bentonite was obtained from natural clay that was high in calcium (NB, State Company of Geological Survey and Mining, Baghdad). The synthesis process used analytical-grade hydrochloric acid (36%) and sodium hydroxide (98%), along with distilled water.

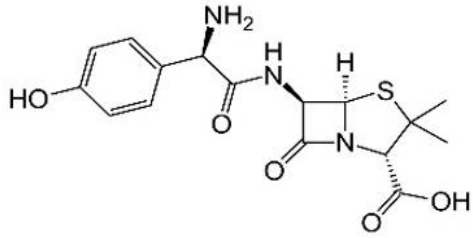

Figure 1. AMOX chemical structure [30]

2.2 Preparation of AMOX stuck solution

The AMOX stock solution was made in distilled water at a concentration of 1000 mg/L. Working solutions ranging from 10 to 80 mg/L were prepared by dilution. Measurements were taken using a UV-Vis spectrophotometer (UV-1100, EMCLAB GmbH, Germany) at 25℃, with absorbance data recorded at 272 nm [31].

2.3 Synthesis of NMgO

Initially, magnesium nitrate solution was created by dissolving half a molar of the salt in 100 milliliters of purified water while stirring continuously for a quarter of an hour to guarantee full dissolution. Thereafter, pH was adjusted and stabilized somewhere between 9 and 10. The amalgam was then left untouched for two hours to permit the reaction to progress suitably. The resultant precipitate was carefully isolated using centrifugation at 4500 revolutions per minute for a quarter of an hour [32]. To boost the purity of the material, repeated washing was done with dH_2O and EtOH. The refined substance was then dried at 100 degrees Celsius for 6 hours. Ultimately, calcination was done at 450℃ for 4 h, adhering to the methodology outlined by the twenty-ninth reference.

2.4 Synthesis of NMgO/bentonite

Iraqi bentonite from its natural state underwent processes to prepare it for composites. Initially, it was purified with distilled water, then dried and broken into small pieces ranging from 250 to 500 micrometers. The granules were then exposed to hydrogen peroxide and were placed in hydrochloric acid for ten hours. Afterward, the now altered clay was rinsed until neutral and dehydrated at a lower heat for half a day, after which it was re-sorted to a smaller 425 micrometer size. The multi-step treatment transformed the raw material into structured components prepared for combination into novel materials. A measured amount of NMgO was dispersed in distilled water using ultrasonication, after which 25 g of bentonite was added and mixed for 60 seconds. Suspension was then autoclaved and thermally treated at 160℃ for 24 h [33]. Filtering, thorough rinsing, and drying at 100℃ for a further 24 hours followed completion. Figure 2 shows the final NMgO-bentonite composite that was made by calcining the material at 450℃ for 5 hours.

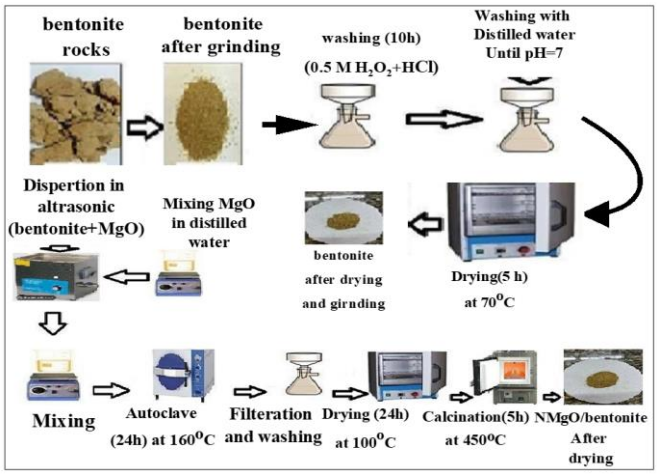

Figure 2. Illustration of the preparation steps of the NMgO/bentonite composite

In order to determine the average size of the NMgO crystallites, this equation [34] was used:

$$D = 0.9\,\lambda/\beta\cos\theta \quad (1)$$

The symbols D, θ, β, and λ represent the average crystallite size, Bragg angle, half maximum full width, and X-ray wavelength, respectively.

2.5 Zero-charge pH (pH_{pzc}) measurement

The surface charge behaviour of untreated bentonite was assessed by preparing multiple flasks containing 0.1 M NaCl solutions, each set to a distinct pH value ranging from 2 to 12. Continuous swirling at room temperature for 48 hours was used to supplement each solution with a 0.1 g NMgO-bentonite composite. After the solid material had been separated by filtration, each sample final pH is calculated. At what pH does the adsorbent surface not have any net charge? This is known as the pH_{pzc}, or point of zero charge. The starting pH is used to get the final pH by charting the difference between the two (ΔpH). The pH_{pzc} line was the same as the plot's x-axis intercept.

2.6 Adsorption process

AMOX removal was evaluated through a series of batch adsorption experiments conducted under different conditions. 100 mL solutions containing 10–80 mg/L AMOX concentrations were mixed with specific dosages of the adsorbent and shaken using a temperature-controlled shaker. Tests were performed at different contact times (10–180 min), pH levels (3–12), agitation speeds (50–350 rpm), and sorbent dosages (0.01–1.5 g/100 mL). At 272 nm, the residual AMOX content was determined using a double-beam UV-V is spectrophotometer (PG Instruments, Model UV T80, England) after filtration through Whatman No. 40 paper had been completed to remove suspended particles. Equilibrium adsorption capacity (q_e, mg/g) was measured via a mass balance approach [35, 36]. The following equations were applied:

$$q_e = \frac{(C_o - C_e)V}{m} \quad (2)$$

$$R(\%) = \frac{(C_o - C_e)}{C_o} \times 100 \quad (3)$$

The adsorbed quantity (mg/g), starting and equilibrium concentrations (mg/L), solution volume (L), adsorbent mass (g), and removal efficiency (R%) are all defined in this context. These expressions provide a quantitative assessment of the adsorption process's efficiency.

There were three separate runs of each experiment, and the standard deviation and the standard error were calculated from the three sets of data to determine the margin of error.

2.7 Adsorption isotherms

Sorption isotherms describe the adsorption mechanism by relating equilibrium concentration to the amount adsorbed at constant temperature [37, 38]. The isotherm models are given below:

$$q_e = \frac{q_m k l C_e}{(1 + k l C_e)} \quad (4)$$

$$R^L = \frac{1}{1 + KlCe} \quad (5)$$

$$q_e = K_F\, C_e^{\frac{1}{n}} \quad (6)$$

$$qe = \frac{KRp\ Ce}{1 + \alpha Ce\hat{}\beta} \quad (7)$$

The Langmuir isotherm model, Eq. (4), which helps describe how matter adheres to surfaces, suggests that adsorption achieves an equilibrium state determined by the interplay between the quantities of adsorbate bonding to the adsorbent. Precisely, it portrays how much of a substance, known as the adsorbate, can affix to a specific mass of material, the adsorbent, quantified in milligrams per gram. This archetype also underscores the maximum amount able to form a solitary coating on the area and presents a constant, Kl that demonstrates how strongly the adsorbate and adsorbent attract one another. The separation factor, R^L in Eq. (5), which indicates the ease of adsorption, is another crucial component: if R^L exceeds one, adsorption isn't preferable; if it lies between zero and one, adsorption is probable; if it equals one precisely, the process is linear; and if R^L is zero exactly, adsorption is irreversible.

Subsequently, the Freundlich isotherm model, Eq. (6), approaches adsorption from an alternative perspective. It relies upon two constants: K_F, which reflects the adsorbent's capacity, and 'n', which denotes how intense and diverse the adsorption operation is across diverse surface regions.

Then, the Redlich–Peterson (RP) in Eq. (7) archetype, which combines notions from both Langmuir and Freundlich models, applies constants like KRP and α, with a factor β ranging from zero to one to depict uneven area.

Fundamentally, the Langmuir model applies best when addressing smooth, uniform surfaces where substances form a single layer. The Freundlich archetype fits more accurately for rough, diverse surfaces. The RP model is adaptable, capturing the intricacies of systems that don't neatly fit into one group or the other.

2.8 Absorption kinetics

The comprehension of how substances adhere to surfaces, a process known as adsorption, is considered fundamental across various scientific disciplines. Kinetic analysis sheds light on this process, especially when subjected to changing circumstances like pressure and temperature. Such analysis is utilized to evaluate the rate and efficiency with which adsorption occurs under divergent circumstances.

Adsorption is not a vacuum process; rather, it is influenced by the characteristics of both the absorbent (the part of the surface that the compound adheres to) and the adsorbate (the substance that is being absorbed). Two principal resistances are identified as potential impediments to this process. The first, external diffusion resistance, can be likened to the difficulty encountered when navigating through a crowded street to reach a specific shop, where the bulk fluid represents the crowd and the shop symbolizes the adsorbent's surface. The second, intraparticle diffusion resistance, resembles the challenge of finding one's way through a large shopping complex after entering the shop, necessitating movement through various departments, analogous to navigating the internal pores, to reach the ultimate destination.

In order to ascertain the primary sources of delay within this process, a variety of models have been developed by scientists. The pseudo-second-order Eq. (9) and the pseudo-first-order Eq. (8) models serve as analytical tools, akin to maps, that facilitate the prediction of the adsorption rate of substances onto surfaces. These models have been extensively applied in the investigation of pharmaceutical compounds, thereby aiding researchers in the optimization of processes to enhance efficiency.

$$qt = q_e\,(1 - e^{-K_1 t}) \tag{8}$$

$$qt = \frac{K_2\, q_e^2 t}{1 + K_2\, q_e^2 t} \tag{9}$$

$$qt = K_d\, t^{0.5} + C \tag{10}$$

$$qt = \frac{1}{\beta}\, ln\,(1 + \alpha\beta t) \tag{11}$$

The amount of solute that the adsorbent is able to collect at a certain moment is known as its adsorption capacity at that time b. Eqs. (8) and (9) show that two separate models were used to study the process kinetics: the pseudo-first-order model, which is characterized by a rate constant K_1 (min^{-1}), and the pseudo-second-order model, which is defined by a rate constant K_2 (g/mg·min). q_e is the equilibrium adsorbed quantity in milligrams per gram, and t is the duration in minutes utilized for kinetic analysis.

Eq. (10), which is part of the intraparticle diffusion model, shows how fast solutes diffuse into adsorbent pores, with K_d ($mg\ g^{-1}\ min^{-1}$) representing the diffusion rate and C representing the thickness of the boundary layer. Chemisorption on heterogeneous surfaces is described by the Elovich model (Eq. (11)), where β is the initial adsorption rate and β is related to activation energy and surface coverage. According to the Arrhenius formula given in Eq. (12) [39]. It was found that the adsorption system's activation energy was 30.35 kJ/mol.

$$k = A\, e^{(-\frac{Ea}{RT})} \tag{12}$$

The formula includes the following variables: k for reaction speed, R for gas constant (8.314 J/mol·K), T for system absolute temperature, Ea for minimum energy necessary for reaction (J/mol), and A is representative of the frequency of successful collisions.

2.9 Thermodynamics study

The adsorption process's thermodynamic properties, such as entropy (ΔS°), enthalpy (ΔH°), and Gibbs free energy (ΔG°), were determined by using Eqs. (13) and (14). These parameters offer a deeper understanding of the spontaneity, thermal behavior, and molecular disorder involved in AMOX adsorption. These parameters are typically derived from temperature-dependent adsorption studies. The equations applied in this analysis followed the approach outlined by the study [40] as follows:

$$\Delta G° = -RTlnkc \tag{13}$$

$$lnKc = \left(\frac{\Delta G°}{RT}\right) = \left(\frac{\Delta S°}{R} - \frac{\Delta H°}{RT}\right) \tag{14}$$

where, Kc is the adsorption equilibrium constant, defined as the amount of AMOX adsorbed on the surface to its concentration in solution. It is a measure of the NMgO-bentonite's affinity for the solute and the solute's mobility in the liquid phase [41].

3. RESULTS AND DISCUSSION

3.1 Characterization of the prepared adsorbent

3.1.1 XRD analysis

With 2θ angles of 36.862°, 42.824°, 62.167°, 74.516°, and 78.443°, respectively, the synthesised NMgO displays six different peaks in its XRD pattern, which correspond to the (111), (200), (220), (311), and (222) crystallographic planes (Figure 3). The XRD results undoubtedly validate the preparation of NMgO [42], aligning with past work by researchers in the field. Moreover, as noted by Ali and Saeideh, the diffraction peaks precisely match the reference card from the JCPDS archives. However, while the pattern agrees with standard profiles, some peaks were broader than expected, revealing minor structural fluctuations. Overall, the crystalline character of the synthesized MgO is soundly established through thorough diffraction analysis, though opportunities remain to refine synthesis methods for increased homogeneity. The sharpness and intensity of the peaks reflect a high degree of crystallinity, which suggests a small particle size and uniform structure.

Figure 4(a, b) displays the patterns created by XRD of the NMgO-bentonite composites both before and during the adsorption process. The sharp, distinct peaks observed suggest a high level of crystallinity, which is probably due to the small particle size of the synthesized Nano MgO. The newly made NMgO-bentonite composite's XRD pattern is shown in Figure 4(a). The 110, 210, 124, and 144 planes of bentonite are aligned with the distinct peaks seen for 2θ values of 20.7°, 26.5°, 36.3°, and 54.7°, which conform to JCPDS card No. 01-088-0891 [43]. In addition, diffraction peaks characteristic of NMgO appear in the composite pattern at the same 2θ positions noted above. These observations confirm the

successful dispersion of MgO nanoparticles onto the bentonite matrix. The synthesized NMgO and NMgO/bentonite samples were found to have average crystallite diameters of 24 nm and 34 nm, respectively. Figure 4(b) presents the XRD pattern of NMgO/bentonite after AMOX adsorption. No significant change in peak intensity was observed. However, slight shifts in peak positions occurred, indicating the interaction of AMOX with the composite surface. This confirms earlier results published by study [44] and indicates that the material maintained its crystalline phase structure after adsorption.

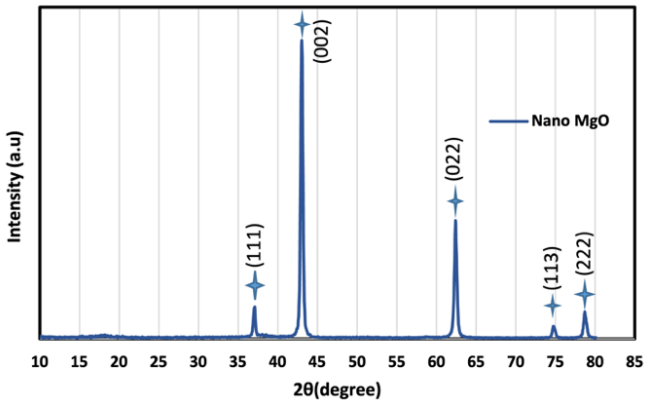

Figure 3. XRD for the prepared NMgO

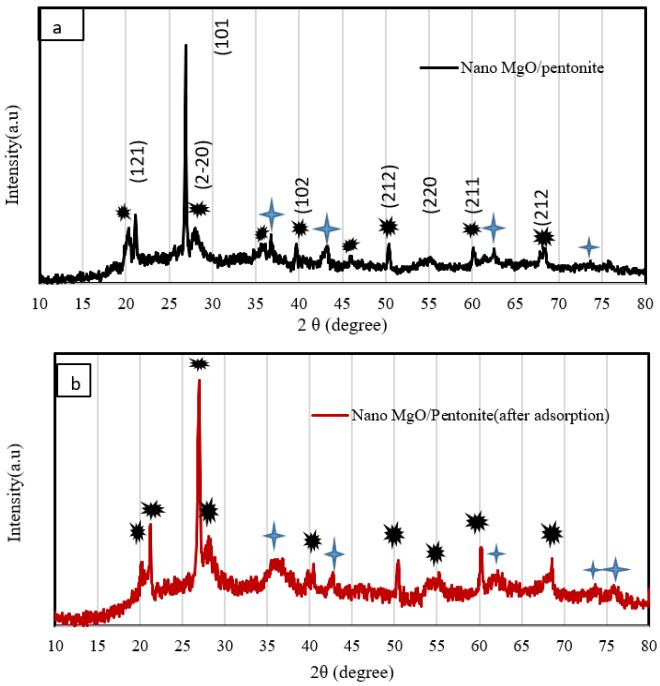

Figure 4. XRD for NMgO/bentonite (a) before and (b) after the adsorption of AMOX

3.1.2 FTIR analysis

Figures 5 and 6 show FTIR spectra of NMgO and NMgO/bentonite, where functional groups were identified before and after AMOX interaction. Using a Bruker Tensor 27 spectrophotometer (USA), spectra were collected in the 400-4000 cm^{-1} range using samples generated using the KBr pellet procedure. Figure 5 shows the FTIR spectrum of synthesized NMgO. Absorption bands between 420 and 862.9 cm^{-1} correspond to metal-oxygen bending vibrations. The band detected between 600 and 850 cm^{-1}, especially in the 700–850 cm^{-1} range, indicates Mg-O and Mg-O-Mg stretching vibrations. These features confirm the successful synthesis of NMgO, in accordance with the intended preparation method.

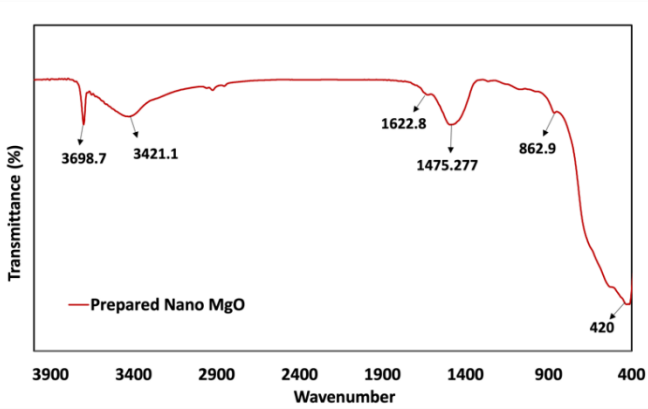

Figure 5. FTIR analysis for synthesized NMgO

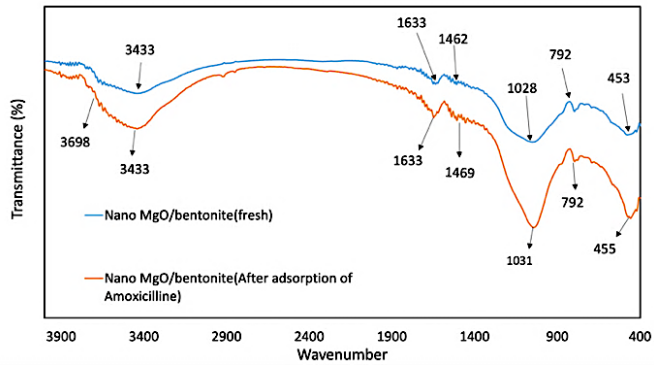

Figure 6. FTIR analysis for NMgO/bentonite before and after adsorption of AMOX

The spectral profile of untreated NMgO/bentonite revealed several characteristic absorption bands. A signal at 457 cm^{-1} confirmed the presence of Si–O bonds, a typical feature of bentonite. The 528 cm^{-1} band corresponds to Mg–O stretching, indicating the MgO phase, while the 646 cm^{-1} band is linked to Al–O bending. The signal recorded at 792 cm^{-1} corresponded to Si–O–Si bonding interactions. An intense band near 1028 cm^{-1} indicated Si–O stretching within the bentonite framework. The 1633 cm^{-1} peak is attributed to C=C stretching and indicates unsaturated hydrocarbons.

Figure 6 also presents the FTIR spectrum of NMgO-bentonite after AMOX adsorption. Several peaks appear shifted or intensified in comparison with the fresh composite. These changes indicate the attachment of AMOX to the adsorbent surface. A wide absorption band noted in the Si–O framework region persists, signifying that the bentonite structure remains intact. The emergence of newer peaks at 1637 cm^{-1} as well as 1654 cm^{-1} indicates the presence of carbonyl groups within the amide bonds, a characteristic sign of AMOX [45]. These peaks' existence confirms possible communications between AMOX molecules and the absorbent surface by validating the existence of amide and carboxylate functional groups. Additionally, the peak seen at 2922 cm^{-1} is actually recognized as corresponding to C–H stretching vibrations, which provide signs of methylene (CH2) and methyl (CH3) groups inside the AMOX arrangement. O-H stretching vibrations are linked to the bands at 3433 cm^{-1} and 3708 cm^{-1}, which suggests that hydroxyl groups on the

NMgO/bentonite surface area and the absorbed AMOX molecules form hydrogen bonds. This peak's presence signals potential interactions involving AMOX substances as well as the adsorbent surface by confirming the actual existence of amide and carboxylate functional groups.

3.1.3 FESEM imaging

The microstructure and surface morphology of bentonite and the NMgO/bentonite composite are shown in Figures 7 and 8, respectively. These images illustrate particles of varying sizes and structural features. Figure 7 displays the morphology of raw bentonite, which appears as irregular flakes marked by surface roughness, ridges, and grooves.

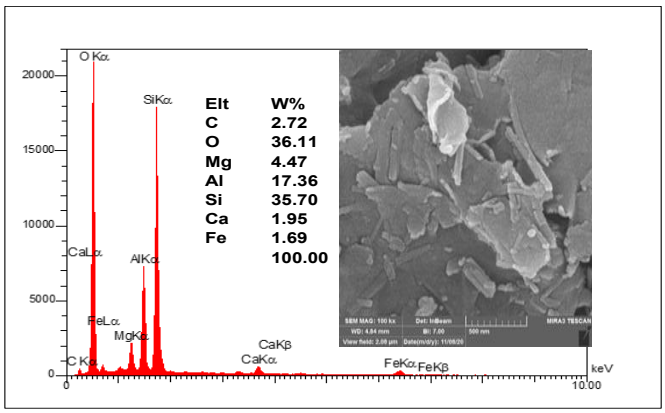

Figure 7. FESEM image and EDX of bentonite

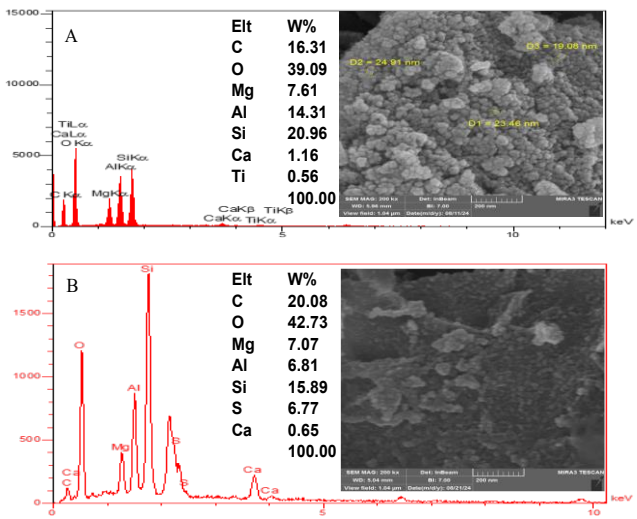

Figure 8. FESEM images and EDX of NMgO-bentonite (A) before and (B) after adsorption of AMOX

Figure 8(A) presents the FESEM image of the prepared NMgO/bentonite composite. The image shows spherical NMgO nanoparticles uniformly distributed across the surface of the bentonite. Micro- and mesoporous structures are visible on the NMgO-bentonite surface, with the MgO coating partially occupying some of the pores. These structural characteristics suggest effective deposition of MgO on the bentonite surface, which may contribute to improved surface reactivity and adsorption performance [46].

Figure 8(B) reveals morphological changes in NMgO-bentonite after the adsorption of AMOX. The composite maintains an overall irregular shape, but a thin layer of adsorbed AMOX is visible on the surface. The layer results in slightly larger particle sizes and a more granular, rough texture. Increased agglomeration is observed, with particle clusters likely forming as a consequence of AMOX adsorption [41]. Small granular deposits present on the NMgO/bentonite surface further confirm the successful attachment of AMOX. The FESEM analysis clearly demonstrates morphological changes after adsorption, which supports the effectiveness of the material as an AMOX adsorbent.

3.2 Evolution of NMgO/bentonite structural parameters

The effectiveness of an adsorbent is determined by a number of parameters, such as specific surface area, total pore volume, and average pore size. The textural features of unmodified bentonite and the NMgO-enhanced composite were assessed using the Brunauer–Emmett–Teller (BET) technique before and after exposure to AMOX, as summarised in Table 1. Results indicated that the NMgO/bentonite composite exhibited a larger surface area than natural bentonite. The increase likely results from the successful dispersion of NMgO particles across the bentonite surface. Pore volume and average pore diameter decreased noticeably after incorporating NMgO into the bentonite. The reduction likely stems from blockages in pores and interlayer channels caused by the minuscule NMgO filling microscopic spaces. Average pore sizes measured approximately eleven and three-quarters nanometers for pure bentonite compared to roughly nine and three-quarters nanometers for the NMgO/bentonite composite, signifying a mesoporous makeup for both materials according to several studies [47]. The decline in the structural values confirms that AMOX molecules occupied the external surface and internal pores (Table 1), as supported by previous studies [48].

Table 1. Surface and structural properties of raw bentonite compared with those of the NMgO-modified composite

Sample	BET Surface Area (m^2/ g)	Pore Volume (cm^3/g)	Average Pore D. (nm)
Bentonite	37.130	0.107	11.57
NMgO/bentonite	57.230	0.052	9.370
After adsorption of AMOX	43.050	0.041	8.739

3.3 Parameters of adsorption

3.3.1 Effect of pH

The heterogeneous character of adsorbents along with the ionization condition of adsorbates at specific pH values, considerably impacts how efficiently a sorption process removes contaminants. A 30 mg/L solution of AMOX was assessed in this investigation across a pH range of 3 to 12. 0.05 g of NMgO/bentonite was utilized as the sorbent, and the solution was gently agitated for two hours at ambient temperature while regulated to move at 200 rpm. Understanding the pH_{pzc}, where the net surface charge becomes zero, is essential for evaluating surface properties and binding interactions.

To increase the adsorption capacity, the adsorbent and the adsorbate must maximise their electrostatic attraction. The surface is positively charged below pH_{Pzc} and negatively charged above it [49]. Figure 9(a) presents the experimental determination of the pH_{pzc} for NMgO/bentonite, which was found to be 7.64. The extent of AMOX adsorption onto

NMgO/bentonite is influenced by the ionization state of AMOX molecules, which is governed by the solution pH. AMOX has three pKa values: 2.4 (carboxylic acid), 7.4 (amine), and 9.6 (phenol). These values determine the dominant ionic species present at distinctive pH levels. The protonation of AMOX is important in determining its adsorption affinity, orientation, and mechanism on different surfaces. The adsorption efficiency of AMOX on NMgO/bentonite (pH_{pzc} = 7.64) is pH-dependent. Adsorption is enhanced by electrostatic interaction between anionic AMOX and positively charged surfaces below pH_{pzc}. Near pH_{pzc}, neutral surfaces favour moderate uptake via hydrogen bonding and van der Waals forces. Above pH_{pzc}, electrostatic repulsion between negatively charged species reduces efficiency.

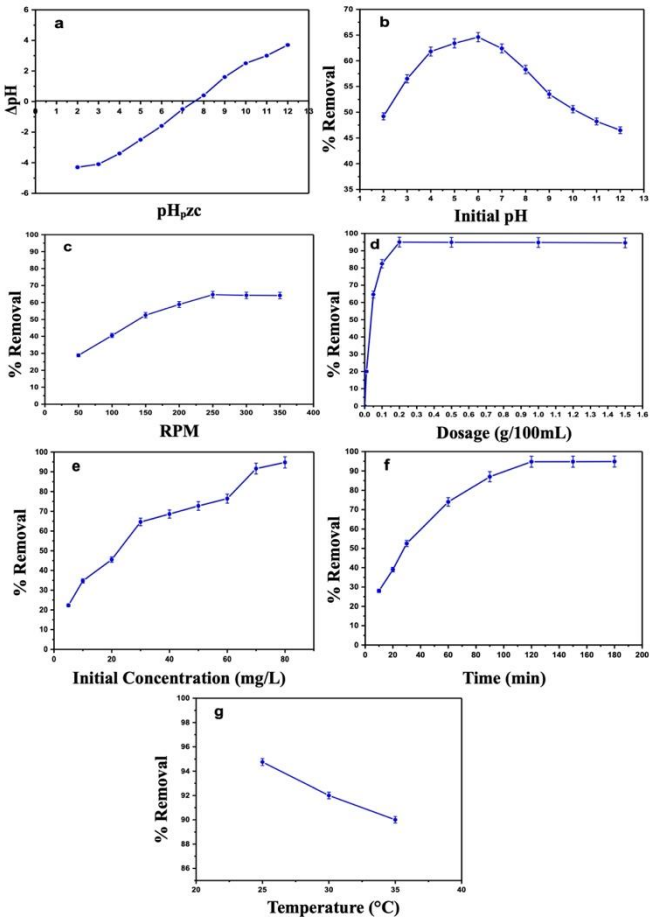

Figure 9. (a) pH_{pzc} of NMgO/bentonite; (b) Effect of pH (C_0 = 30 mg/L, t = 2 h, m = 0.05 g, V = 100 mL, 200 rpm); (c) Effect of agitation speed (C_0 = 30 mg/L, t = 2 h, m = 0.05 g, pH = 6, V = 100 mL); (d) Effect of dose (t = 2 h, pH = 6, V = 100 mL, 250 rpm); (e) Effect of contact time (C_0 = 80 mg/L, m = 0.2 g, pH = 6, V = 100 mL, 250 rpm); (f) Effect of initial concentration (m = 0.2 g, t = 2 h, pH = 6, V = 100 mL, 250 rpm); (g) Effect of temperature (C_0 = 80 mg/L, m = 0.2 g, t = 2 h, pH = 6, V = 100 mL)

At a pH of 6, the removal efficiency peaked at 64.6% (Figure 9(b)), and it continued to rise as the pH ranged from 3 to 6. However, further raising the pH beyond this level resulted in decreased adsorption efficiency. Under acidic conditions, AMOX predominantly carries a positive charge because of protonation at its amino and phenolic functional groups. During this condition, the surface of the adsorbent also tends to exhibit a positive charge, which leads to electrostatic repulsion that reduces adsorption efficiency. Maximum adsorption occurred at pH 6, near the pH_{pzc} of NMgO/bentonite, where the surface was nearly neutral and interacted more effectively with AMOX. Adsorption effectiveness decreased as the surface became more negatively charged at acidic pH due to electrostatic repulsion [50].

3.3.2 Effect of agitation speed

The agitation speed has a significant impact on the efficiency of the adsorption process; in fact, there is an ideal agitation speed for each adsorbent material. Figure 9(c) presents the influence of agitation speeds on AMOX removal using NMgO/bentonite. Initial studies demonstrated that as the rate of stirring elevated, the amount of AMOX eliminated also grew dramatically. While some sentences in the report were rather brief, other portions went into more thorough explanation [51]. For instance, it delved into how the improved productivity might be due to amplified disturbance, which trims the boundary layer thickness encircling the absorbent bits and boosts the handoff of mass. The maximum removal capacity was accomplished at two hundred fifty revolutions per minute, determined as the most excellent agitation speed for the NMgO/bentonite composite, given its ability to propagate turbulence and facilitate transfer.

3.3.3 Effect of dosage

Removal capacity and effectiveness of adsorption are significantly influenced by the quantity of adsorbent utilized. The influence of various dosages on AMOX removal was evaluated within the range of 0.01 to 1.5 g, as exhibited in Figure 9(d). It was discerned that increasing the amount of adsorbent resulted in enhanced removal proficiency, with optimal output observed at a dosage of 0.2 g per 100 mL of solution. The adsorption effectiveness dropped with successive increments, indicating that the adsorbent surface's active sites were saturated.

When concentrations are increased, overlapping or diminution of the effective surface area of these locations may transpire, thereby diminishing potency [52]. Conversely, when lower amounts are used, the active sites remain more accessible, thereby boosting the performance of the adsorbent. An augmentation in the quantity of adsorbent also intensifies particulate collisions, which can lead to the liberation of formerly absorbed ions back into the solution, a process termed desorption. Furthermore, excessive dosage can cause particle aggregation and the development of overlapping layers. Such structural modifications increase the distance between adsorption sites and AMOX molecules in solution, thereby decreasing overall adsorption capacity [53, 54].

3.3.4 Effect of initial concentration

Investigating how different initial concentrations of AMOX affect the system offers valuable information about the material's adsorption capacity. Figure 9(e) presents the percentage of AMOX removed at various starting concentrations. Higher initial AMOX concentration resulted in a greater removal percentage at equilibrium. Such a trend is explained by the rise in mass transfer driving force, which promotes greater molecular movement toward the adsorbent surface until saturation of active sites occurs [55].

The increased availability of AMOX molecules enhances binding at the adsorbent surface, particularly at active sites, because of the forces of electrostatic attraction and van der

Waals. However, as the concentration continues to rise, the ratio of removed AMOX decreases. The decline in AMOX removal reflects the increasing gap between initial and final concentrations and shows that available adsorption sites were insufficient to accommodate the excess solute [56].

3.3.5 Effect of contact time

The effectiveness of AMOX removal using NMgO/bentonite as an adsorbent is significantly influenced by the contact duration. The experimental data indicate a steady increase in the removal percentage within the 5 to 180-minute time frame (Figure 9(f)). The abundance of active sites enabled rapid adsorption initially and maintained a high AMOX removal rate up to 120 min. Nevertheless, the adsorption rate decreases when these active sites are saturated. Beyond this point, diffusion of AMOX into the adsorbent core controlled the process [57, 58]. Maximum removal was reached after 2 h of agitation. Beyond this point, further contact time offered no measurable improvement in performance and confirmed that equilibrium had been reached.

3.3.6 Effect of temperature

The adsorption performance of NMgO/bentonite for AMOX was evaluated at different temperatures. Figure 9(g) presents the experimental results. A relationship was observed between temperature and AMOX removal efficiency. At 30°C and 35°C, the removal rate decreased, indicating a decline in adsorption efficiency at elevated temperatures. A decrease in the binding strength of AMOX molecules to the adsorbent surface might be the cause of the performance drop. At higher temperatures, adsorbed molecules were released into the solution, which reduced adsorption capacity and removal efficiency [59].

3.4 Adsorption isotherms

Adsorption isotherms clarified the interaction between AMOX and the NMgO/bentonite surface at equilibrium. Table 2 shows that the fitted parameters, high R^2 values, and low SSE confirmed the suitability of all three models. Figure 10 further elucidates how adsorption capacity fluctuates across changing equilibrium concentrations.

Table 2. Comparison between isotherm models

Langmuir		Freundlich		Redlich–Peterson (R-P)	
q_{max}	263.143	KF	1.2	K_{R-P}	0.620
K_L	0.024	n	2.12	α	0.00034
R_L	0.838	1/n	0.471	β	0.65
SSE	1.111	SSE	1.111	SSE	1.116
R^2	0.979	R^2	0.981	R^2	0.979

The experimental findings correspond closely with all three isotherm models, evidenced by the likeness in R^2 and SSE values. This coherency implies that AMOX's adsorption onto NMgO/bentonite likely involves a combination of consistent and divergent surface interactions, denoting mono- and multi-layer adsorption systems at work [50]. In particular, the Freundlich model exhibited the highest R^2, indicating that heterogeneous, multi-layer interactions on the surface mainly impact the process [51]. Meanwhile, the parameters K_L, R_L, and β all fall inside recognized scopes conducive to adsorption—K_L between 0 and 1, 1/n less than 0.5, and β between 0 and 1—affirming NMgO/bentonite's effectiveness as an AMOX adsorbent [60]. The results confirmed strong binding between the surface and AMOX. As postulated by the Langmuir model, maximum adsorption transpires once AMOX forms a uniform monolayer, completely masking the available surface sites. The theory assumes consistent adsorption energy across these sites, precluding lateral movement or interactions [53]. The BET surface area of NMgO/bentonite measured 57.23 m^2/g, which represents a moderate increase over the 37.13 m^2/g recorded for raw bentonite. Despite this modest difference in surface area, the maximum adsorption capacity of the NMgO-modified material reached 263.23 mg/g, significantly surpassing the 26 mg/g observed for bentonite alone. Calculated adsorption site densities further support this discrepancy, with NMgO/bentonite showing approximately 7.57×10^{18} sites/m^2, while bentonite exhibits only 1.15×10^{18} sites/m^2. This significant difference suggests that adsorption performance is governed primarily by the nature, density, and accessibility of chemically active sites rather than total surface area measured by physical adsorption of inert gases [60].

Table 3. Comparison of AMOX adsorption capacities across different materials

Adsorbent	q_m (mg/g)	Reference
Magnetic Graphene Oxide Nanocomposite	98.41	[61]
Chemically treated olive stone was used as the precursor material for producing activated carbon	67.7	[62]
Activated carbon was produced using olive biomass as the precursor, with $ZnCl_2$ applied as the activating agent.	237.02	[63]
Thermal treatment was performed in a conventional muffle furnace.	166.96	
Acid-Activated Biochar	239.230	[64]
Breadfruit seed hull biochar	61.02	[65]
breadfruit seed hull biochar modified using ZnO-NPs	49.82	
Bentonite-chitosan composite	86.1	[66]
Modified bentonite using chemical and physical methods	21.8818 13.7362	[67]
Nano MgO/bentonite	263.143	**This Work**

where q_m is obtained using the Langmuir constant

A range of previously reported materials has been evaluated against the NMgO/bentonite composite to contextualize its AMOX uptake performance. The comparative adsorption capacities are outlined in Table 3. The comparison highlights the superior performance of NMgO/bentonite relative to other synthetic adsorbents. The enhanced removal efficiency of NMgO/bentonite suggests a synergistic interaction between its components, contributing to its excellent adsorption capabilities. These findings indicate that NMgO/bentonite holds significant potential for water treatment applications and may attract considerable attention in future research and practical implementations.

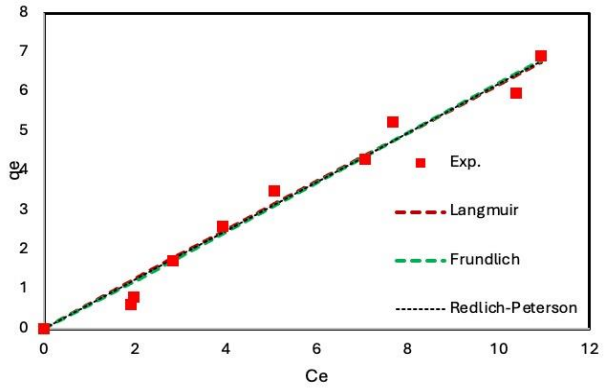

Figure 10. Comparison of experimental data with the q_e values derived from the isotherm models for AMOX using Nano MgO/bentonite

3.5 Absorption kinetics

Figure 11 and Table 4 illustrate the kinetic modelling outcomes for AMOX adsorption onto NMgO/bentonite. Among the models assessed, Correlation values of 0.996 for the Elovich equation and 0.989 for the pseudo-second-order equation indicated the best match, respectively, for the experimental data. The strong alignment between the experimental adsorption capacity (q_e, exp = 68.55 mg/g) and the pseudo-second-order model's predicted value (q_e, cal = 68.9 mg/g) further confirms its effectiveness in describing the adsorption mechanism [68].

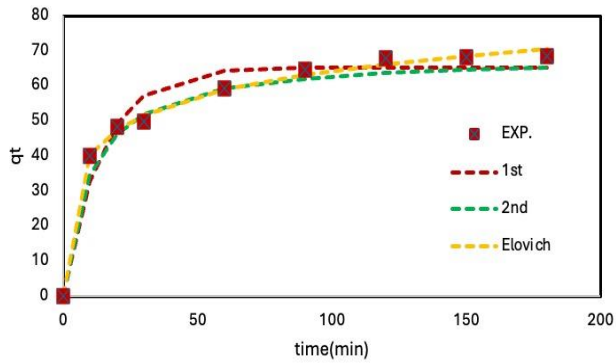

Figure 11. Adsorption kinetic models for the adsorption of AMOX onto NMgO/bentonite

Table 4. Kinetic model parameters for AMOX adsorption on NMgO–bentonite

Model	Parameter	AMX
Pseudo first order	q_e (mg/g)	65
	K_1 (min^{-1})	0.898
	SSE	19.819
	R^2	0.960
Pseudo-second order	q_e	68.9
	K_2 (g mg^{-1} min^{-1})	0.0015
	SSE	10.29
	R^2	0.989
Intra-particle diffusion	K_{IP}	2.813
	C	34.822
	SSE	14.044
	R^2	0.996
Elovich	α	47.135
	β	0.096
	SSE	14.044
	R^2	0.996

In accordance with the intraparticle diffusion concept, Figure 12 displays a linear relationship between q_e and $t^{0.5}$. The slope and intercept gave K_{ip} and C. Since the line veered away from the origin, it was determined that intraparticle diffusion was a factor, but it was not the limiting one [69]. The initial AMOX concentration and the related K_{ip} values show a favorable connection in Table 4. The pattern suggests that boundary layer diffusion controlled the rate-limiting step [70].

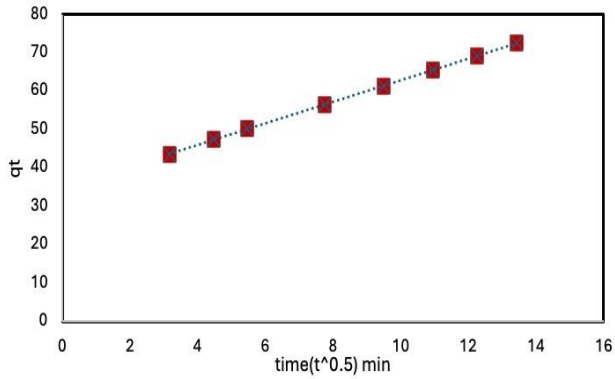

Figure 12. Intra-particle model for adsorption of AMOX onto NMgO/bentonite

3.6 Thermodynamics study

In order to determine ΔH° and ΔS°, the slope and intercept were obtained from a linear plot of ln Kc vs 1/T, Eq. (14), as shown in Figure 13. These values were then used to determine ΔG° (Table 5). Negative ΔS° and ΔG° values verified spontaneity and decreased disorder at the solid-liquid interface, respectively. The ΔH° value of –43 kJ/mol, consistent with previous reports [71-74], suggested an exothermic process driven by chemisorption.

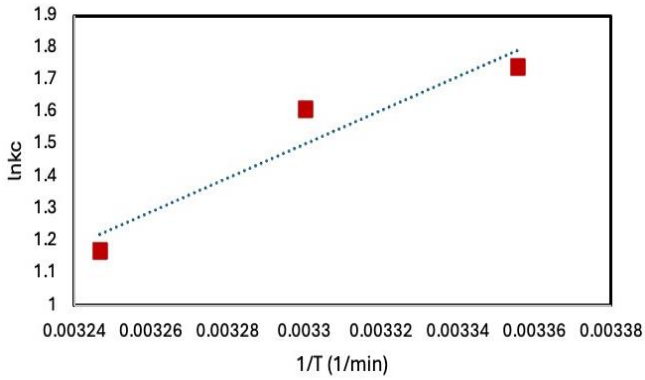

Figure 13. Thermodynamics of AMOX onto NMgO/bentonite

Table 5. Thermodynamic parameters for AMOX adsorption onto NMgO/bentonite

Temp.(k)	ΔG°	ΔH°	ΔS°	R^2
298	-4.441			
303	-3.786	-43.850	-0.131	0.908
308	-3.131			

3.7 Reusability of NMgO/bentonite

The reusability of NMgO/bentonite was evaluated under controlled conditions across six consecutive adsorption–

regeneration cycles (Figure 12). Post each adsorption cycle, the used adsorbent underwent regeneration through washing with 1 M acetone, dried for 24 hours at 50°C after rinsing with double-distilled water. Figure 14 demonstrates a steady decrease in adsorption efficiency across multiple regeneration cycles. The loss in performance may result from leaching of active components into the washing solution, structural alterations in the adsorbent, and a reduction in surface area and pore availability. After six reuse cycles, the adsorption capacity decreased by only 9.35%, which confirms that NMgO/bentonite maintains its effectiveness for AMOX removal even after multiple regeneration steps.

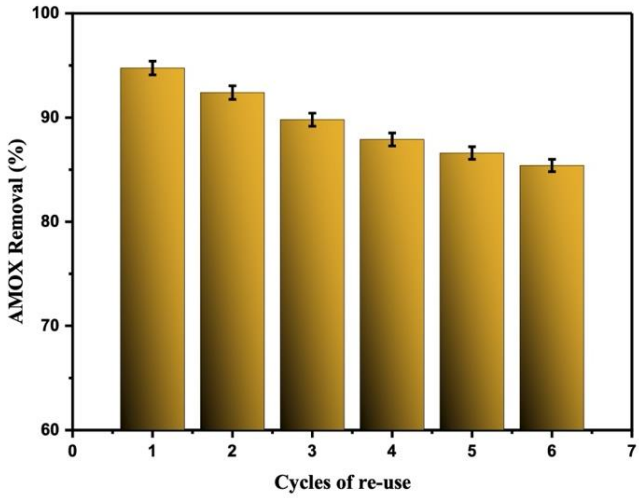

Figure 14. Reusability of NMgO/bentonite

3.8 Economic analysis

An economic evaluation was performed to determine the practicality of applying bentonite and MgO as sorbents for removing AMOX from water. The highest adsorption capacity was measured at 263.143 mg/g, with a starting concentration of 80 mg/L. Calculations indicated that approximately 0.3041 kg of the adsorbent would be needed to purify 1000 litres (1 ton) of contaminated solution. The treatment cost was found to be highly economical: approximately $0.046 when using NMgO/bentonite. The findings show that NMgO/bentonite is a cost-effective solution for treating pharmaceutical pollutants in large-scale water treatment systems. The analysis showed that NMgO/bentonite removed emerging pollutants effectively and offered a low-cost, practical solution.

4. CONCLUSIONS

Characterization analyses confirmed that the NMgO and NMgO/bentonite composites were effectively synthesized in this work, accomplishing the desired preparation goals. The materials demonstrated an impressive 94% AMOX removal effectiveness when optimized at pH 6, 425 µm particle size, 250 rpm agitation speed, 2 g/L dose, 120 minutes contact time, and temperature at 25°C. Variation in solution pH significantly influenced the adsorption efficiency. Freundlich was the best-fitting model, which indicated a non-uniform surface and suggested multilayer adsorption. The Langmuir model indicated that the maximal adsorption capacity was 263.143 mg/g. Kinetic analysis suggested that the dominant mechanism involved chemical interactions. The pseudo-second-order model had the strongest correlation ($R^2 = 0.989$) with the experimental data. The process's exothermic nature was shown using thermodynamic analysis, which verified that it happened spontaneously and released heat. After six regeneration cycles with 1 M acetone, reusability tests showed only a 9.35% reduction in performance, indicating the NMgO/bentonite composite's continued effectiveness even after repeated usage. The results confirmed that the composite outperformed other adsorbents in AMOX removal and reusability. It is advised that further research examine the composite's effectiveness in actual wastewater conditions, selectivity in complicated mixes, and performance in continuous flow systems.

REFERENCES

[1] Almontasser, A., Parveen, A., Azam, A. (2019). Synthesis, characterization and antibacterial activity of magnesium oxide (MgO) nanoparticles. IOP Conference Series: Materials Science and Engineering, 577(1): 012051. https://doi.org/10.1088/1757-899X/577/1/012051

[2] Abdulkareem, H.N., Alwared, A.I. (2019). Immobilization dried mix of algae for copper removal. Iraqi Journal of Agricultural Sciences, 50(3): 800-808.

[3] Munzhelele, E.P., Mudzielwana, R., Ayinde, W.B., Gitari, W.M. (2024). Pharmaceutical contaminants in wastewater and receiving water bodies of South Africa: A review of sources, pathways, occurrence, effects, and geographical distribution. Water, 16(6): 796. https://doi.org/10.3390/w16060796

[4] Ahmed, S.F., Mofijur, M., Nuzhat, S., Chowdhury, A.T., et al. (2021). Recent developments in physical, biological, chemical, and hybrid treatment techniques for removing emerging contaminants from wastewater. Journal of Hazardous Materials, 416: 125912. https://doi.org/10.1016/j.jhazmat.2021.125912

[5] Samal, K., Mahapatra, S., Ali, M.H. (2022). Pharmaceutical wastewater as Emerging Contaminants (EC): Treatment technologies, impact on environment and human health. Energy Nexus, 6: 100076. https://doi.org/10.1016/j.nexus.2022.100076

[6] Yin, H., Ren, Z., Gao, H., Han, W., Guan, J. (2021). Preparation of amphoteric modified bentonite from calcium-based bentonite for adsorption of anionic dye. The importance of sodium-modification pretreatment. Physicochemical Problems of Mineral Processing, 57(1): 1-17. https://doi.org/10.37190/ppmp/127920

[7] Hummadi, K.K., Luo, S., He, S. (2022). Adsorption of methylene blue dye from the aqueous solution via bio-adsorption in the inverse fluidized-bed adsorption column using the torrefied rice husk. Chemosphere, 287: 131907. https://doi.org/10.1016/j.chemosphere.2021.131907

[8] Faisal, A.A., Abdul-Kareem, M.B., Mohammed, A.K., Ghfar, A.A. (2021). Novel sorbent of sand coated with humic acid-iron oxide nanoparticles for elimination of copper and cadmium ions from contaminated water. Journal of Polymers and the Environment, 29(11): 3618-3635. https://doi.org/10.1007/s10924-021-02132-3

[9] Jamel, A.A.J., Dawood, Z.T. (2024). Generation rainfall intensity equations for intensity duration frequency (IDF)

curves (Case study: Salah Al-Din, Iraq). Instrumentation, Mesures, Métrologies, 23(4): 265-275. https://doi.org/10.18280/i2m.230402

[10] Hasan, Y.R., Shaban, M.A.A., Ibrahim, M.A., M-Ridha, M.J., Hussein, H.A. (2023). Effect of calcination temperature on the adsorption performance of Mg/Al layered double hydroxide nanoparticles in the removal of meropenem antibiotics. Iraqi Journal of Agricultural Sciences, 54(1): 42-58. https://doi.org/10.36103/ijas.v54i1.1675

[11] Tahar, A., Choubert, J.M., Miège, C., Esperanza, M., Le Menach, K., Budzinski, H., Wisniewski, C., Coquery, M. (2014). Removal of xenobiotics from effluent discharge by adsorption on zeolite and expanded clay: An alternative to activated carbon? Environmental Science and Pollution Research, 21(8): 5660-5668. https://doi.org/10.1007/s11356-013-2439-6

[12] Girish, C.R., Murty, V.R. (2015). Adsorption of phenol from aqueous solution using Lantana camara, forest waste: Packed bed studies and prediction of breakthrough curves. Environmental Processes, 2(4): 773-796. https://doi.org/10.1007/s40710-015-0117-z

[13] Hummadi, K.K. (2021). Optimal operating conditions for adsorption of heavy metals from an aqueous solution by an agriculture waste. Iraqi Journal of Chemical and Petroleum Engineering, 22(2): 27-35. https://doi.org/10.31699/IJCPE.2021.2.4

[14] Aranda, F.L., Rivas, B.L. (2022). Removal of amoxicillin through different methods, emphasizing removal by biopolymers and its derivatives. An overview. Journal of the Chilean Chemical Society, 67(3): 5643-5655. https://doi.org/10.4067/S0717-97072022000305643

[15] De Ilurdoz, M.S., Sadhwani, J.J., Reboso, J.V. (2022). Antibiotic removal processes from water & wastewater for the protection of the aquatic environment-A review, Journal of Water Process Engineering, 45: 102474. https://doi.org/10.1016/j.jwpe.2021.102474

[16] Khoshnamvand, N., Ahmadi, S., Mostafapour, F.K. (2017). Kinetic and isotherm studies on ciprofloxacin an adsorption using magnesium oxide nanopartices. Journal of Applied Pharmaceutical Science, 7(11): 79-83. https://doi.org/10.7324/JAPS.2017.71112

[17] Huang, R., Liu, Q., Huo, J., Yang, B. (2017). Adsorption of methyl orange onto protonated cross-linked chitosan. Arabian Journal of Chemistry, 10(1): 24-32. https://doi.org/10.1016/j.arabjc.2013.05.017

[18] Sun, W.J., Tang, Q.T., Lu, T.H., Fan, R.D., Sun, G.G., Tan, Y.Z. (2024). Adsorption performance of bentonite and clay for Zn (II) in landfill leachate. Geoenvironmental Disasters, 11: 4. https://doi.org/10.1186/s40677-023-00265-2

[19] Wydro, U., Wołejko, E., Luarasi, L., Puto, K., Tarasevičienė, Ž, Jabłońska-Trypuć, A. (2023). A review on pharmaceuticals and personal care products residues in the aquatic environment and possibilities for their remediation. Sustainability, 16(1): 169. https://doi.org/10.3390/su16010169

[20] Perelomov, L., Gertsen, M., Burachevskaya, M., Hemalatha, S., Vijayalakshmi, A., Perelomova, I., Atroshchenko, Y. (2024). Organoclays based on bentonite and various types of surfactants as heavy metal remediants. Sustainability, 16(11): 4804. https://doi.org/10.3390/su16114804

[21] Mubarak, M.F., Selim, H., Hawash, H.B., Hemdan, M. (2024). Flexible, durable, and anti-fouling maghemite copper oxide nanocomposite-based membrane with ultra-high flux and efficiency for oil-in-water emulsions separation. Environmental Science and Pollution Research, 31(2): 2297-2313. https://doi.org/10.1007/s11356-023-31240-x

[22] Ortiz-Ramos, U., Leyva-Ramos, R., Mendoza-Mendoza, E., Aragón-Piña, A. (2022). Removal of tetracycline from aqueous solutions by adsorption on raw Ca-bentonite. Effect of operating conditions and adsorption mechanism. Chemical Engineering Journal, 432: 134428. https://doi.org/10.1016/j.cej.2021.134428

[23] Alexander, J.A., Ahmad Zaini, M.A., Surajudeen, A., Aliyu, E.N.U., Omeiza, A.U. (2019). Surface modification of low-cost bentonite adsorbents—A review. Particulate Science and Technology, 37(5): 538-549. https://doi.org/10.1080/02726351.2018.1438548

[24] Ghoniem, M.G., Ben Aissa, M.A., Ali, F.A.M., Khairy, M. (2022). Efficient and rapid removal of Pb(II) and Cu(II) heavy metals from aqueous solutions by MgO nanorods. Inorganics, 10(12): 256. https://doi.org/10.3390/inorganics10120256

[25] Alghanmi, R.M., Abdelrahman, E.A. (2024). Simple production and characterization of ZnO/MgO nanocomposite as a highly effective adsorbent for eliminating congo red dye from water-based solutions. Inorganic Chemistry Communications, 161: 112137. https://doi.org/10.1016/j.inoche.2024.112137

[26] Guo, Y., Zhou, Z., Alshabrmi, F.M. (2024). Efficiency of magnesium oxide nanoparticle in contaminants removal from environmental water samples: Optimization through central composite design. Chemosphere, 362: 141734. doi.org/10.1016/j.chemosphere.2024.141734

[27] Selvam, N.C.S., Kumar, R.T., Kennedy, L.J., Vijaya, J.J. (2011). Comparative study of microwave and conventional methods for the preparation and optical properties of novel MgO-micro and nano-structures. Journal of Alloys and Compounds, 509(41): 9809-9815. https://doi.org/10.1016/j.jallcom.2011.08.032

[28] Hussein, M.F., Mubarak, M.F., Al-Sirhani, A.M., Hosny, R. (2024). Examining the factors that impact the formation of barite scale in water injection operations: experimental study and quantification of scale formation. Discover Applied Sciences, 6(10): 519. https://doi.org/10.1007/s42452-024-06176-7

[29] Liu, Y., Zhu, K., Wang, J., Huang, X., Wang, G., Li, C., Cao, J., Ding, S. (2016). Simultaneous detection and comparative pharmacokinetics of amoxicillin, clavulanic acid and prednisolone in cows' milk by UPLC–MS/MS. Journal of Chromatography B, 1008:74-80. https://doi.org/10.1016/j.jchromb.2015.11.031

[30] De Marco, B.A., Natori, J.S.H., Fanelli, S., Tótoli, E.G., Salgado, H.R.N. (2017). Characteristics, properties and analytical methods of amoxicillin: A review with green approach. Critical Reviews in Analytical Chemistry, 47(3): 267-277. https://doi.org/10.1080/10408347.2017.1281097

[31] Alardhi, Y.T.D.K.T. (2024). The relationship between basic psychological needs, novelty, and transformative experience: A cross-cultural study. Doctoral dissertation, University of Northern Colorado, https://digscholarship.unco.edu/dissertations/1079.

[32] Elkhatib, I., Nogueira, D., Bayram, A., Abdala, A., Del Gallego, R., Melado, L., Munck, N., Lawrenz, B., Fatemi, H. (2023). How to identify patients who would benefit from delayed-matured oocytes insemination: A sibling oocyte and ploidy outcome study. Human Reproduction,38(8): 1473-1483. doi.org/10.1093/humrep/dead129.

[33] Hamad, M.T.M.H. (2023). Optimization study of the adsorption of malachite green removal by MgO nano-composite, nano-bentonite and fungal immobilization on active carbon using response surface methodology and kinetic study. Environmental Sciences Europe, 35: 26. https://doi.org/10.1186/s12302-023-00728-1

[34] Aldabagh, I.S., Hummadi, K.K. (2024). Comprehensive characterization for efficient adsorption of Tetracycline from wastewater from the synthesis of nanoparticles by batch and fluidized bed column. Environmental Advances, 19: 100606. https://doi.org/10.1007/s10924-021-02132-3

[35] Mullassery, M.D., Fernandez, N.B., Anirudhan, T.S. (2015). Adsorptive removal of acid red from aqueous solutions by cationic surfactant-modified bentonite clay. Desalination and Water Treatment, 56(7): 1929-1939. https://doi.org/10.1080/19443994.2014.958110

[36] Hummadi, K.K., Zhu, L., He, S. (2023). Bio-adsorption of heavy metals from aqueous solution using the ZnO-modified date pits. Scientific Reports, 13(1): 22779. https://doi.org/10.1007/s10924-021-02132-3.

[37] Goyi, A.A., Sher Mohammad, N.M., Omer, K.M. (2024). Preparation and characterization of potato peel derived hydrochar and its application for removal of Congo red: a comparative study with potato peel powder. International Journal of Environmental Science and Technology, 21(1): 631-642. doi.org/10.1007/s13762-023-04965-y

[38] Hummadi, K.K., Mohammed, A.H.A., Elaibi, A.I., Ali, S.M., Heeres, H.J., He, S. (2020). Catalytic conversion of furfural extract from lubricating oil extraction unit over the shaped and promoted HY catalysts to valuable petroleum products. Catalysis Communications, 134: 105834. https://doi.org/10.1016/j.catcom.2019.105834

[39] Šimon, P., Dubaj, T., Cibulková, Z. (2024). An alternative to the concept of variable activation energy. Journal of Thermal Analysis and Calorimetry, 149(20): 11507-11516. https://doi.org/10.1007/s10973-023-12711-2

[40] Lin, S.H., Juang, R.S. (2009). Adsorption of phenol and its derivatives from water using synthetic resins and low-cost natural adsorbents: A review. Journal of Environmental Management, 90(3): 1336-1349. https://doi.org/10.1016/j.jenvman.2008.09.003

[41] Chai, J.B., Au, P.I., Mubarak, N.M., Khalid, M., Ng, W.P.Q., Jagadish, P., Walvekar, R., Abdullah, E.C. (2020). Adsorption of heavy metal from industrial wastewater onto low-cost Malaysian kaolin clay–based adsorbent. Environmental Science and Pollution Research, 27(12): 13949-13962. https://doi.org/10.1007/s10924-021-02132-3

[42] Xi, H., Shulha, H.P., Lin, J.M., Vales, T.R., et al. (2007). Identification and characterization of cell type-specific and ubiquitous chromatin regulatory structures in the human genome. PLoS Genetics, 3(8): e136. https://doi.org/10.1371/journal.pgen.0030136

[43] Ahmed, M.B., Zhou, J.L., Ngo, H.H., Guo, W., Johir, M.A.H., Belhaj, D. (2017). Competitive sorption affinity of sulfonamides and chloramphenicol antibiotics toward functionalized biochar for water and wastewater treatment. Bioresource Technology, 238: 306-312. https://doi.org/10.1016/j.biortech.2017.04.042

[44] Saucier, C., Karthickeyan, P., Ranjithkumar, V., Lima, E.C., dos Reis, G.S., de Brum, I.A.S. (2017). Efficient removal of amoxicillin and paracetamol from aqueous solutions using magnetic activated carbon. Environmental Science and Pollution Research, 24(6): 5918-5932. https://doi.org/10.1007/s11356-016-8304-7

[45] Sim, H.T., Gençaslan, M., Merdan, M. (2024). Synthesis of MgO nanoparticles via the sol-gel method for antibacterial applications, investigation of optical properties and comparison with commercial MgO. Discover Applied Sciences, 6: 577. https://doi.org/10.1007/s42452-024-06299-x

[46] Malenica, M., Vukomanović, M., Kurtjak, M., Masciotti, V., et al. (2021). Perspectives of microscopy methods for morphology characterisation of extracellular vesicles from human biofluids. Biomedicines, 9(6): 603. https://doi.org/10.3390/biomedicines9060603

[47] Zha, S.X., Zhou, Y., Jin, X.Y., Chen, Z.L. (2013). The removal of amoxicillin from wastewater using organobentonite. Journal of Environmental Management, 129: 569-576. https://doi.org/10.1016/j.jenvman.2013.08.032

[48] Belaissa, Y., Saib, F., Trari, M. (2022). Removal of amoxicillin in aqueous solutions by a chemical activated carbons derived from Jujube nuts: Adsorption behaviors, kinetic and thermodynamic studies. Reaction Kinetics, Mechanisms and Catalysis, 135(2): 1011-1030. https://doi.org/10.1007/s11144-022-02159-0

[49] Shang, Z., Hu, Z., Huang, L., Guo, Z., Liu, H., Zhang, C. (2020). Removal of amoxicillin from aqueous solution by zinc acetate modified activated carbon derived from reed. Powder Technology, 368: 178-189. https://doi.org/10.1007/s10924-021-02132-3

[50] Kasirajan, R., Bekele, A., Girma, E. (2022). Adsorption of lead (Pb-II) using CaO-NPs synthesized by solgel process from hen eggshell: Response surface methodology for modeling, optimization and kinetic studies. South African Journal of Chemical Engineering, 40: 209-229. https://doi.org/10.1016/j.sajce.2022.03.008

[51] Fito, J., Abewaa, M., Mengistu, A., Angassa, K., Ambaye, A.D., Moyo, W., Nkambule, T. (2023). Adsorption of methylene blue from textile industrial wastewater using activated carbon developed from Rumex abyssinicus plant. Scientific Reports, 13(1): 5427. https://doi.org/10.1038/s41598-023-32341-w

[52] Tibebu, S., Kassahun, E., Ale, T.H., Worku, A., et al. (2024). The application of Rumex Abysinicus derived activated carbon/bentonite clay/graphene oxide/iron oxide nanocomposite for removal of chromium from aqueous solution. Scientific Reports, 14(1): 19280. https://doi.org/10.1038/s41598-024-70238-4

[53] Atta, H.A., Hummadi, K.K., M-Ridha, M.J. (2023). A sustainable raw rice husk adsorbent for effective levofloxacin removal from aqueous solution: Kinetic, thermodynamic and isotherm studies. Iraqi Journal of Agricultural Sciences, 54(5): 1407-1420. https://doi.org/10.36103/ijas.v54i5.1841

[54] Radha, E., Gomathi, T., Sudha, P.N., Latha, S., Ghfar, A. A., Hossain, N. (2025). Adsorption studies on removal of Pb (II) and Cd (II) ions using chitosan derived copoymeric blend. Biomass Conversion and Biorefinery, 15(2): 1847-1862. https://doi.org/10.1007/s13399-021-01918-8

[55] Atta, H.A., Hummadi, K.K., M-Ridha, M.J. (2022). The application of response surface methodology and Design-Expert® for analysis of ciprofloxacin removal from aqueous solution using raw rice husk: Kinetic and isotherm studies. Desalination and Water Treatment, 248: 203-216. https://doi.org/10.5004/dwt.2022.28074

[56] Chaba, J.M., Nomngongo, P.N. (2019). Effective adsorptive removal of amoxicillin from aqueous solutions and wastewater samples using zinc oxide coated carbon nanofiber composite. Emerging Contaminants, 5: 143-149. https://doi.org/10.1016/j.emcon.2019.04.001

[57] Kumar, V. (2019). Adsorption kinetics and isotherms for the removal of rhodamine B dye and Pb+ 2 ions from aqueous solutions by a hybrid ion-exchanger. Arabian Journal of Chemistry, 12(3): 316-329. https://doi.org/10.1016/j.arabjc.2016.11.009

[58] Davoudinejad, M., Ghorbanian, S.A. (2013). Modeling of adsorption isotherm of benzoic compounds onto GAC and introducing three new isotherm models using new concept of Adsorption Effective Surface (AES). Scientific Research and Essays, 8(46): 2263-2275. https://doi.org/10.5897/SRE10.643

[59] Amrutha, Jeppu, G., Girish, C.R., Prabhu, B., Mayer, K. (2023). Multi-component adsorption isotherms: review and modeling studies. Environmental processes, 10(2): 38. https://doi.org/10.1007/s40710-023-0063noor1-0

[60] Ortiz-Ramos, U., Leyva-Ramos, R., Mendoza-Mendoza, E., Carrasco-Marín, F., Bailón-García, E., Villela-Martínez, D.E., Valdez-García, G.D. (2024). Modeling adsorption rate of Trimethoprim, tetracycline and chlorphenamine from aqueous solutions onto natural bentonite clay. Elucidating mass transfer mechanisms. Chemical Engineering Journal, 493: 152666. https://doi.org/10.1016/j.cej.2024.152666

[61] Mostafapour, F.K., Bazi, M., Siddiqui, S.H., Bagheri, H., Balarak, D. (2021). Highly efficient adsorption and removal of amoxicillin from aqueous solution by magnetic graphene oxide nanocomposite. International Journal of Pharmaceutical Investigation, 11(4): 384-388. https://doi.org/10.5530/ijpi.2021.4.69

[62] Limousy, L., Ghouma, I., Ouederni, A., Jeguirim, M. (2017). Amoxicillin removal from aqueous solution using activated carbon prepared by chemical activation of olive stone. Environmental Science and Pollution Research, 24: 9993-10004. https://doi.org/10.1007/s11356-016-7404-8.

[63] Rodrigues, D.L.C., Machado, F.M., Osório, A.G., de Azevedo, C.F., et al. (2020). Adsorption of amoxicillin onto high surface area–activated carbons based on olive biomass: Kinetic and equilibrium studies. Environmental Science and Pollution Research, 27: 41394-41404. https://doi.org/10.1007/s11356-020-09583-6

[64] Adu-Poku, D., Saah, S.A., Sakyi, P.O., Bandoh, C.K., et al. (2024). Acid-activated biochar for efficient elimination of amoxicillin from wastewater. Journal of Chemistry, 2024(1): 3648098. https://doi.org/10.1155/2024/3648098

[65] Amaku, J.F., Mtunzi, F.M. (2024). Adsorption of amoxicillin onto breadfruit seed hull biochar modified using ZnONPs: Disinfection and decontamination. Biomass Conversion and Biorefinery, 15: 14369-14385. https://doi.org/10.1007/s13399-024-06313-7

[66] Yeo, J.Y.J., Khaerudini, D.S., Soetaredjo, F.E., Waworuntu, G.L., Ismadji, S., Putranto, A., Sunarso, J. (2023). Experimental and modelling study of adsorption isotherms of amoxicillin, ampicillin and doripenem on bentonite-chitosan composite. South African Journal of Chemical Engineering, 43(1): 38-45. https://doi.org/10.1016/j.sajce.2022.09.013

[67] Naji, A.M., Abd Ali, Z.T. (2023). Evaluation of modified bentonite using chemical and physical methods for removal of amoxicillin from aqueous solutions: Batch and continuous study. Desalination and Water Treatment, 294: 185-201. https://doi.org/10.5004/dwt.2023.29564.

[68] Ragab, A.H., Mettwally, B.S., Mubarak, M.F., Al-Ghamdi, A., Hemdan, M. (2024). Eco-friendly Electrospinning of Recycled Nylon 6, 12 Waste for High-Performance Nonwoven Nanofibers in Sustainable Textile Applications. Journal of Inorganic and Organometallic Polymers and Materials, 34(4): 1491-1505. https://doi.org/10.1007/s10924-021-02132-3

[69] Noor, M.H.M., Ngadi, N. (2024). Global research landscape on coagulation-flocculation for wastewater treatment: A 2000–2023 bibliometric analysis. Journal of Water Process Engineering, 64: 105696. https://doi.org/10.1007/s10924-021-02132-3

[70] Tran, H.N. (2023). Applying linear forms of pseudo-second-order kinetic model for feasibly identifying errors in the initial periods of time-dependent adsorption datasets. Water, 15(6): 1231. https://doi.org/10.1007/s10924-021-02132-3

[71] El Miz, M., Akichoh, H., Berraaouan, D., Salhi, S., Tahani, A. (2017). Chemical and physical characterization of Moroccan bentonite taken from Nador (north of Morocco). American Journal of Chemistry, 7(4): 105-112. https://doi.org/10.5923/j.chemistry.20170704.01

[72] Shelash Al-Ha-Wary, S.I., Gupta, R., Sapaev, I.B., et al. (2025). Efficient removal of amoxycillin antibiotics onto magnetic graphene oxide: Adsorption performance, mechanism, and regeneration exploration. International Journal of Environmental Analytical Chemistry, 105(3): 558-580. https://doi.org/10.1080/03067319.2023.2266698

[73] Hemdan, M., Ragab, A.H., Elyan, S.S., Taher, M.A., Mubarak, M.F. (2025). Eco-friendly activated carbon thin film-zeolitic imidazolate framework-8 (ACTF@ ZIF-8) nanocomposite for efficient methylene blue removal: Synthesis, characterization, and adsorption performance. Journal of Cluster Science, 36(1): 2. https://doi.org/10.1007/s10876-024-02730-w

[74] Aldabagh, I.S., Hummadi, K.K. (2024). Effectiveness and analysis of synthesis nanoparticles walnut shells/zinc oxide to reduce trimethoprim from aqueous solutions. Case Studies in Chemical and Environmental Engineering, 9: 100674. https://doi.org/10.1016/j.cscee.2024.100674